Available online at www.sciencedirect.com

SCIENCE DIRECT®

Earth and Planetary Science Letters 223 (2004) 187–202

EPSL

www.elsevier.com/locate/epsl

Crustal structure of the northern margin of the eastern Tien Shan, China, and its tectonic implications for the 1906 M~7.7 Manas earthquake

Chun-Yong Wang[a], Zhu-En Yang[b], Hai Luo[a], W.D. Mooney[c,*]

[a] Institute of Geophysics, China Seismological Bureau, Beijing 100081, China
[b] Institute of Geology, China Seismological Bureau, Beijing 100029, China
[c] U.S. Geological Survey, Earth Quake Hazards Team, 345 Middlefield Road. MS.977, Menlo Park, CA 94025, USA

Received 24 September 2003; received in revised form 12 April 2004; accepted 13 April 2004

Abstract

The Tien Shan orogenic belt is the most active intracontinental mountain belt in the world. We describe an 86-km-long N–S-trending deep seismic reflection profile (which passes through the southern Junggar basin) located on the northeastern Tien Shan piedmont. Two distinct anticlines beneath the northern margin of the Tien Shan are clearly imaged in the seismic section. In addition, we have imaged two detachment surfaces at depths of ~7 and ~16 km. The detachment surface at 16-km depth corresponds to the main detachment that converges with the steep angle reverse fault (the Junggar Southern Marginal Fault) on which the 1906 M~7.7 Manas earthquake occurred. A 12–14-km-thick sedimentary basin is imaged beneath the southern Junggar basin near Shihezi. The crust beneath the northern margin of the Tien Shan is 50–55-km thick, and decreases beneath the Junggar basin to 40–45-km thick. The crustal image of the deep seismic reflection profile is consistent with models derived from nearby seismic refraction data and Bouguer gravity anomalies in the same region. The faulting associated with the 1906 Manas earthquake also fits within the structural framework imaged by the seismic reflection profile. Present-day micro-seismicity shows a hypocentral depth-distribution between 5 and 35 km, with a peak at 20 km. We hypothesize that the 1906 Manas earthquake initiated at a depth of ~20 km and propagated upwards, causing northward slip on the sub-horizontal detachments beneath the southern Junggar basin. Thus, in accord with regional geological mapping, the current shortening within the eastern Tien Shan is accommodated both by high-angle reverse faulting and detachment faulting that can be clearly imaged at depth in seismic reflection data.
Published by Elsevier B.V.

1. Introduction

The Tien Shan orogenic belt, the most active intracontinental mountain belt in the world, extends in an east–west direction for some 2500 km across central Asia (Fig. 1a). It is located between the Tarim basin to the south and the stable Kazakh platform to the north. The western and central Tien Shan (alternate spelling: Tian Shan), with topography locally exceeding 7 km, is more than 300-km wide and lies mainly within Kyrgyzstan and China. The eastern Tien Shan, discussed here, is located northeast of the

* Corresponding author. Tel.: +1-650-329-4764; fax: +1-650-329-5163.
E-mail address: mooney@usgs.gov (W.D. Mooney).

0012-821X/$ - see front matter. Published by Elsevier B.V.
doi:10.1016/j.epsl.2004.04.015

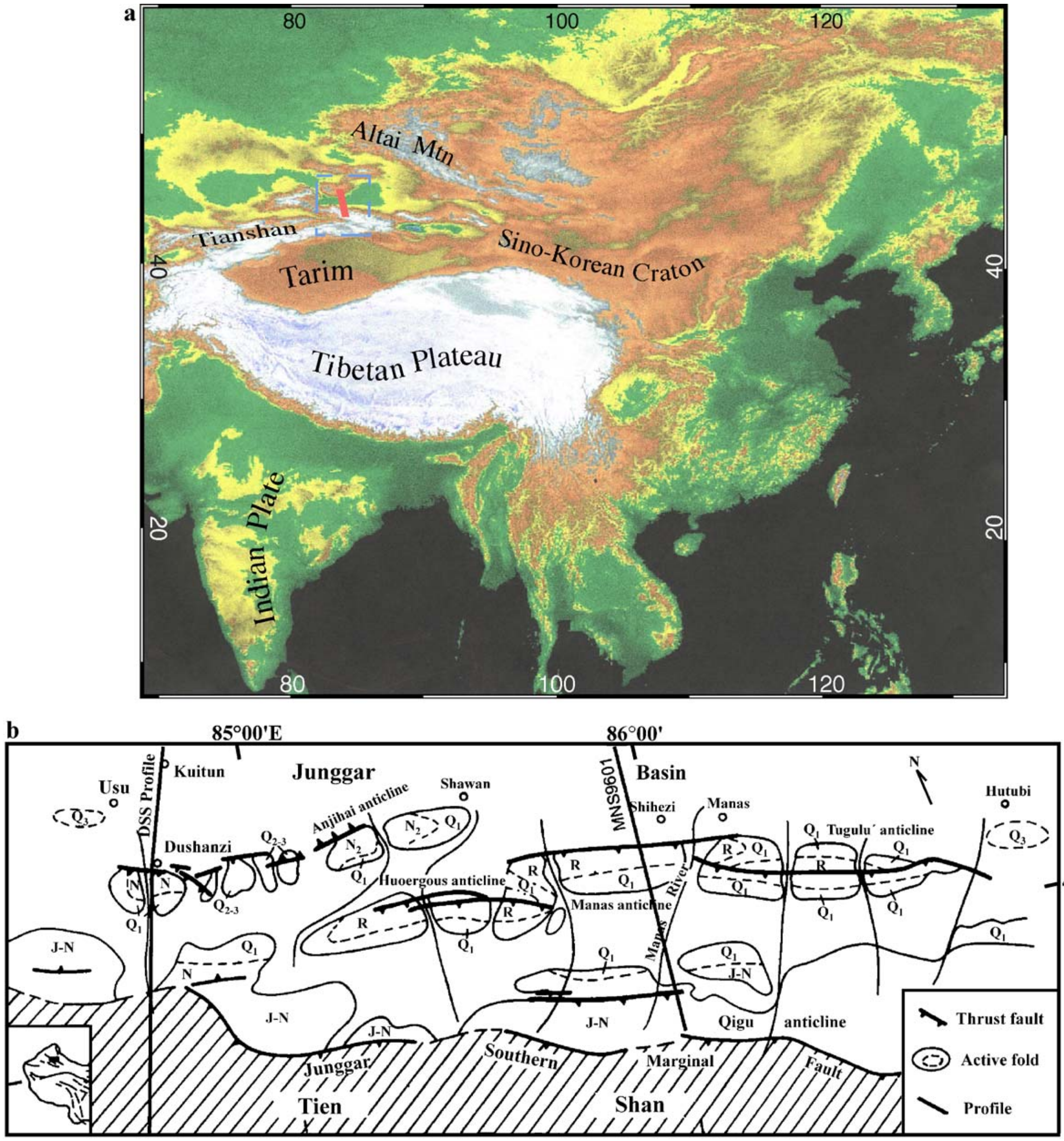

Fig. 1. (a) Tectonic setting of the Tien Shan in northwest China. The blue box outlines the study area while the red line marks the location of the profile; (b) Geologic setting of the northern margin of the Tien Shan and southern Junggar basin (from [22]). The N–S deep seismic reflection profile MNS9601 described in this paper is located near 86°E. In addition, we present data from the N–S deep seismic sounding profile near 85°E that passes through Kuitun and Dushanzi. Key place names in the vicinity of the seismic reflection profile are provided in Fig. 4.

Tarim basin, and is narrower and lower in elevation. Crustal amalgamation and stabilization of the Tien Shan and neighboring geologic provinces dates to the middle and late Paleozoic, when fragments of continental, island arc, and passive continental margin crust coalesced to form southern Eurasia (e.g., [1,2]). The entire orogen was reactivated as a result of the continental collision of India with Asia, with the front of the active collision zone located some 1500 km to the south of the Tien Shan [3,4].

Although this collision began at ~ 55 Ma, recent detailed studies have documented that the uplift of the present-day Tien Shan has occurred only in the past ~ 20 Ma, with most of the uplift occurring during the past 7–11 Ma [5–11]. GPS data indicate that the present-day shortening rate across the western Tien Shan may be as high as ~ 23 mm/year, and may accommodate as much as 50% of the total shortening between India and the Siberian platform [46] [12–14]. In our study area, the central Tien Shan, the shortening rate is on the order of 6 mm/year, as determined from GPS data [13], Holocene kinematics [15] and balanced sections [7]. As a result of this ongoing deformation, this region has a high level of seismic activity, with magnitude>5 earthquakes concentrated along the southern and northern margins of the Tien Shan. Nodal planes document reverse faulting dipping at angles of 30° to 60° (Fig. 2) [16–19]. Over the last century, a series of strong earthquakes have occurred on the margins of the Tien Shan, including the 1906 magnitude ~ 7.7 Manas earthquake [20], located on the northern margin, and the 1949 magnitude ~ 7.2 Luntai earthquake, located on the southern margin (Fig. 2). Geological and geophysical investigations (e.g., [7,10,15–17,21,22]) have attempted to tie these strong earthquakes to the tectonics study in this region. In order to better constrain the tectonics of

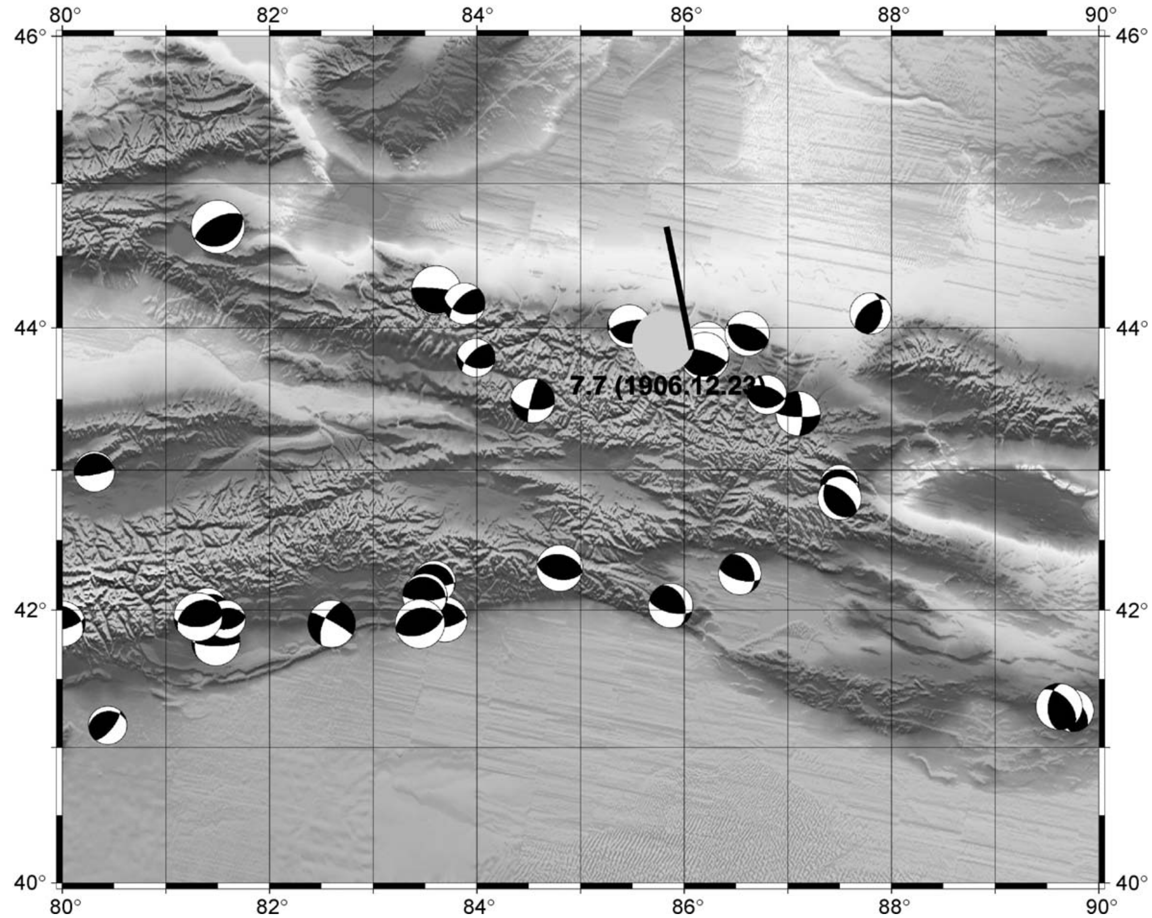

Fig. 2. Focal mechanisms determined by first arrivals in the local network for the eastern Tien Shan [44]. The 1906 M~7.7 Manas earthquake (large open circle) is associated with several events showing reverse-faulting solutions. The interior of the Tien Shan has a lower level of seismicity than the northern and southern margins. The MNS9601 seismic reflection profile is shown as a solid black line.

this region, we carried out a deep seismic reflection survey at the northern margin of the Tien Shan that passed through the epicentral area of the 1906 Manas earthquake (Fig. 1b). We present a seismic image of the crustal structure along this profile and discuss its interpretation in terms of the accommodation of crustal shortening in this region. We also discuss the possible relation of our seismic image to the faulting associated with the 1906 Manas earthquake.

2. Regional geologic setting and location of the deep seismic reflection profile

Three sub-parallel sets of reverse faults and fold belts have developed in the Cenozoic strata of the Ürümqi Depression of the northern piedmont of the Tien Shan [7,15] (Molnar et al., 1994). From south to north, they are the Qigu, Huoergous–Manas–Tugulu and Dushanzi–Anjihai reverse fault/fold belts (Fig. 1b). Each of these fold belts takes the form of an asymmetric anticline, with the gentle slope to the south, and the steeper slope to the north. Reverse faults, with the hanging wall to the south, are associated with the northern flank of each fold. Such active fold belts have developed at large scales in this region since the middle Miocene [7,10]. Some of the folds have formed over blind thrusts, but in most cases the basal thrust fault has reached the surface where it cuts and offsets river terraces [15]. Thus, field evidence shows that fault slip has occurred along the major reverse faults associated with these anticlines. River terraces have been folded and deformed in the valleys flowing from the Tien Shan into the Junggar basin. The deformation of lower terraces demonstrates that active deformation has continued through the Holocene [15,18,21,22].

Abundant earthquake epicenters are distributed throughout the entire Tien Shan, but magnitude ≥ 5.0 earthquakes in the Tien Shan tend to be concentrated along its southern and northern margins (Fig. 2) [16,17]. Since 1716, historical data show that 78 earthquakes with magnitude ≥ 5.0 have occurred in the northern seismic belt of the Tien Shan. Three of these earthquakes are estimated to have had a magnitude greater than 7.0. In particular, the 1906 Manas

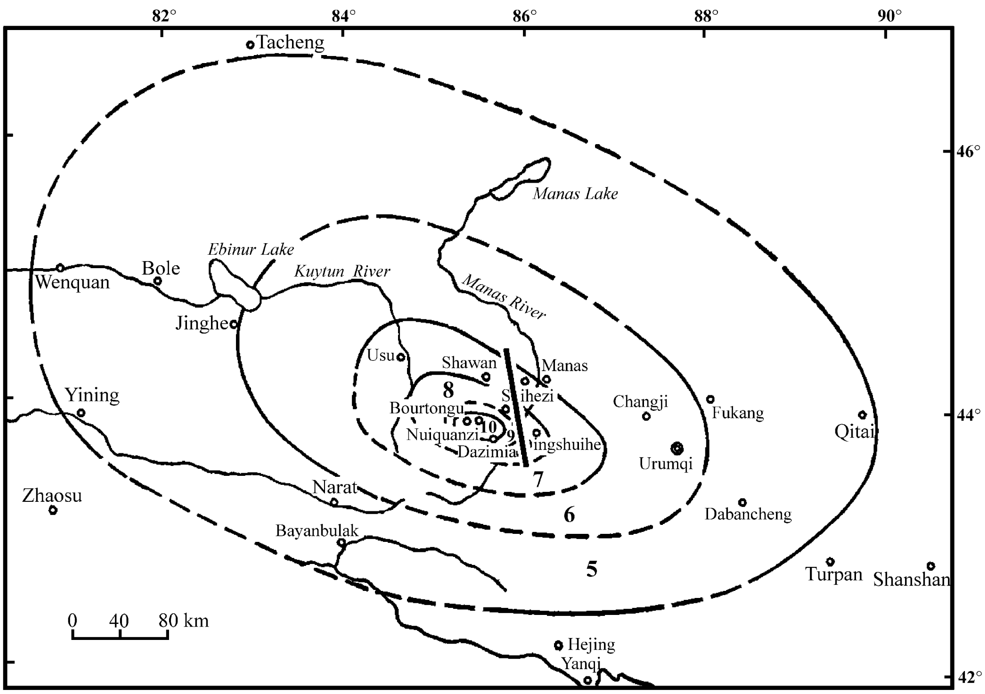

Fig. 3. Isoseismal map of the 1906 Manas M~7.7 earthquake and location of the MNS9601 deep seismic reflection profile.

earthquake (magnitude ~7.7) occurred within this seismic belt. Since 1970, when a regional seismic network was deployed in the Xinjiang Uygur Autonomous Region, 16 earthquakes with magnitude ≥ 5.0 have occurred. The epicenter of the Manas earthquake is located at 43.9°N, 85.6°E (Figs. 3 and 4) [23]. Based on the isoseismal map (Fig. 3), the east–west trending Qingshuihe fault is inferred to be the fault on which the Manas earthquake occurred. Burchfiel et al. [7] discuss the tectonic setting and uncertainty in magnitude of the Manus earthquake.

In this paper, we present an 86-km-long deep seismic reflection profile that crosses the northern margin of the eastern Tien Shan, through the epicentral area of the 1906 Manas earthquake (Fig. 3). The profile trends NNW across the depression of the Ürümqi piedmont zone. The profile begins at the northern margin of the Tien Shan, crosses the Qing-

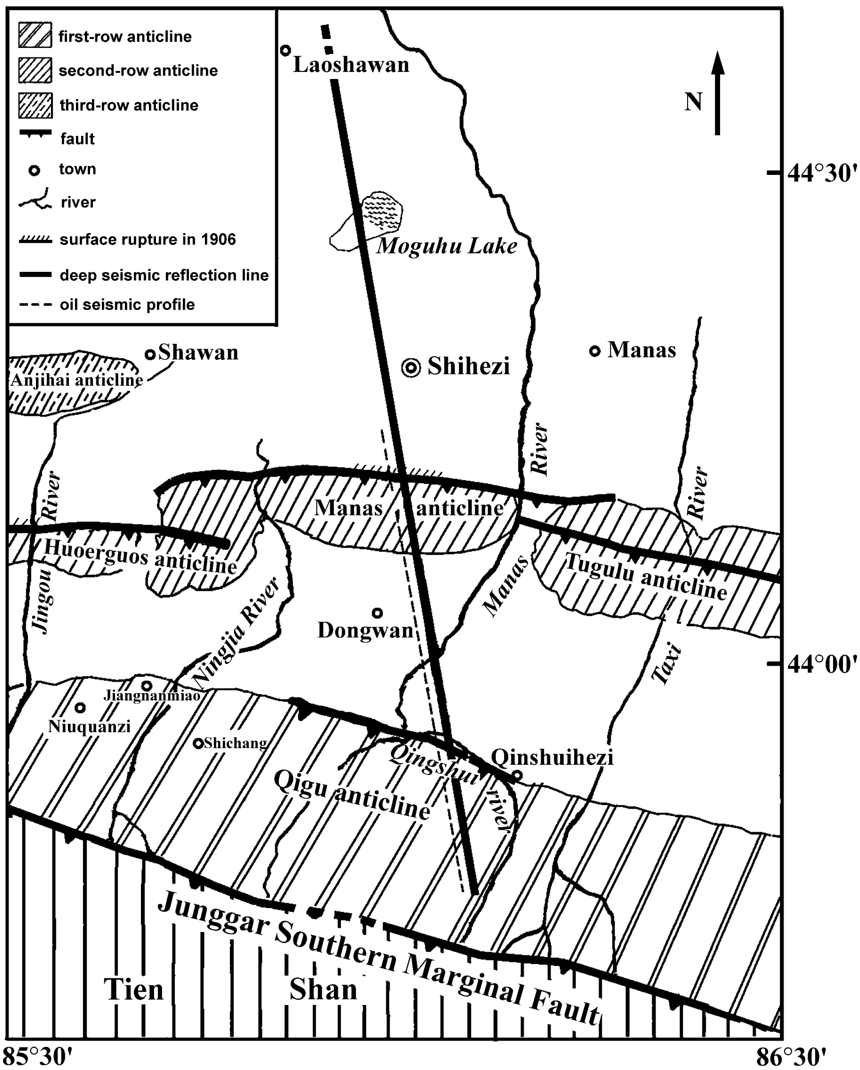

Fig. 4. Geologic setting and location of the seismic reflection profile. The epicenter of the 1906 Manas M~7.7 earthquake is shown as a dark circle. Note that surface ruptures were mapped following the 1906 earthquake. The Manas and Qigu anticlinal structures [45] depicted here form an important part of our analysis.

shuihe and Manas rivers, the Manas valley and Manas anticline, and ends at the desert margin of the Junggar basin (Fig. 4). We refer to this reflection profile as MNS9601 throughout this paper.

3. Data acquisition and processing

The data acquisition for the MNS9601 reflection profile was completed using a truck-mounted 240-channel, 24-bit digital telemetry EAGLE seismograph, which is produced by OPSEIS Inc. in the United States. The acquisition system consists of a central recording unit and seismic acquisition stations. A split spread with composite detection was used. The acquisition parameters in the field were as follows: a geophone group interval of 100 m, a minimum offset of 500 m, 24-fold coverage, a sample interval of 4 ms, and a 24-s record length.

The recorded seismic data were processed using the following techniques: field static correction, deconvolution, velocity analysis, residual static correction, normal moveout correction (NMO) and/or dipping moveout correction (DMO), and stacking. The static correction and the velocity analysis were especially important in the data processing of the profile. Static corrections were applied to numerous seismic profiles from the Xinjiang region. The velocity structure determined from deep seismic sounding data [24], taken in the northern Tien Shan, was used for the stacking velocity for two-way travel times (TWT) >5 s.

4. Image of fine crustal structure

A line drawing of the CDP stacked section for profile MNS9601 is shown in Fig. 5. We describe the features of the crust seen in this seismic section (the upper and middle crust, lower crust, and crust–mantle transition) in the following discussion.

4.1. Upper and middle crust

Along the southern portion of the profile, the surface elevation decreases from south to north, and a set of shallow reflections with low-angle northward dip is evident (Figs. 5 and 6a). These reflections correlate with the north-dipping South Qingshuihe reverse fault. To the north of these reflections is another branch of the Qingshuihe fault, this one with a southward dip; this fault is less evident in the seismic reflection data than the clearly-imaged low-angle northward dipping faults (Fig. 6a). The inferred inclinations of the Qingshuihe faults also differ from that of the strata at the surface. In addition, there is a

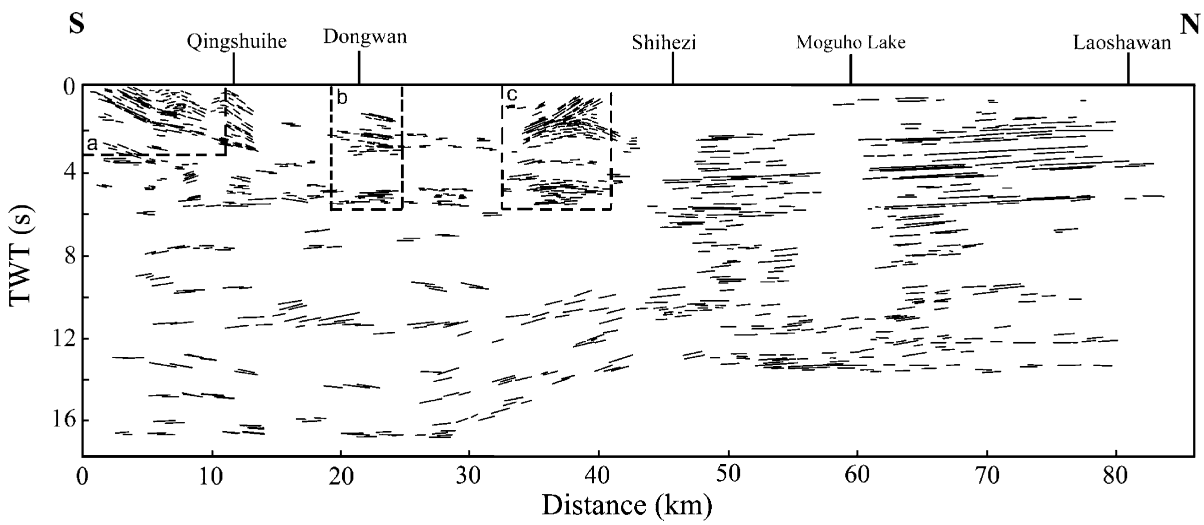

Fig. 5. Synthesis of the main observations from this MNS9601 seismic reflection profile. This line drawing was made from the CDP stacking section. Labels a, b and c in the dash-line frames indicate data shown in Fig. 6a, b, and c.

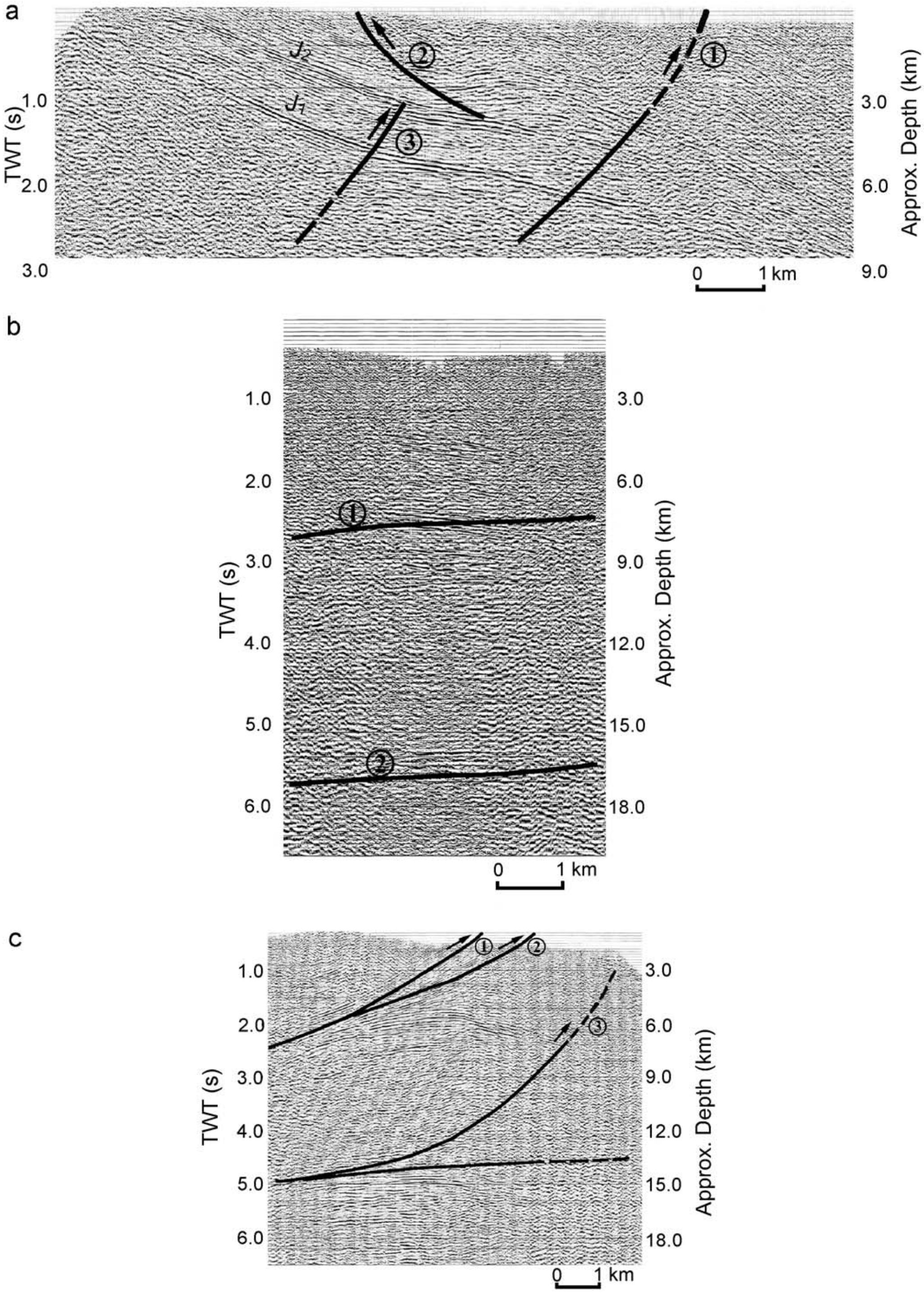
a
J2
J1
1.0
2.0
3.0
TWT (s)
3.0
6.0
9.0
Approx. Depth (km)
0 1 km
b
1.0
2.0
3.0
4.0
5.0
6.0
TWT (s)
3.0
6.0
9.0
12.0
15.0
18.0
Approx. Depth (km)
0 1 km
c
1.0
2.0
3.0
4.0
5.0
6.0
TWT (s)
3.0
6.0
9.0
12.0
15.0
18.0
Approx. Depth (km)
0 1 km

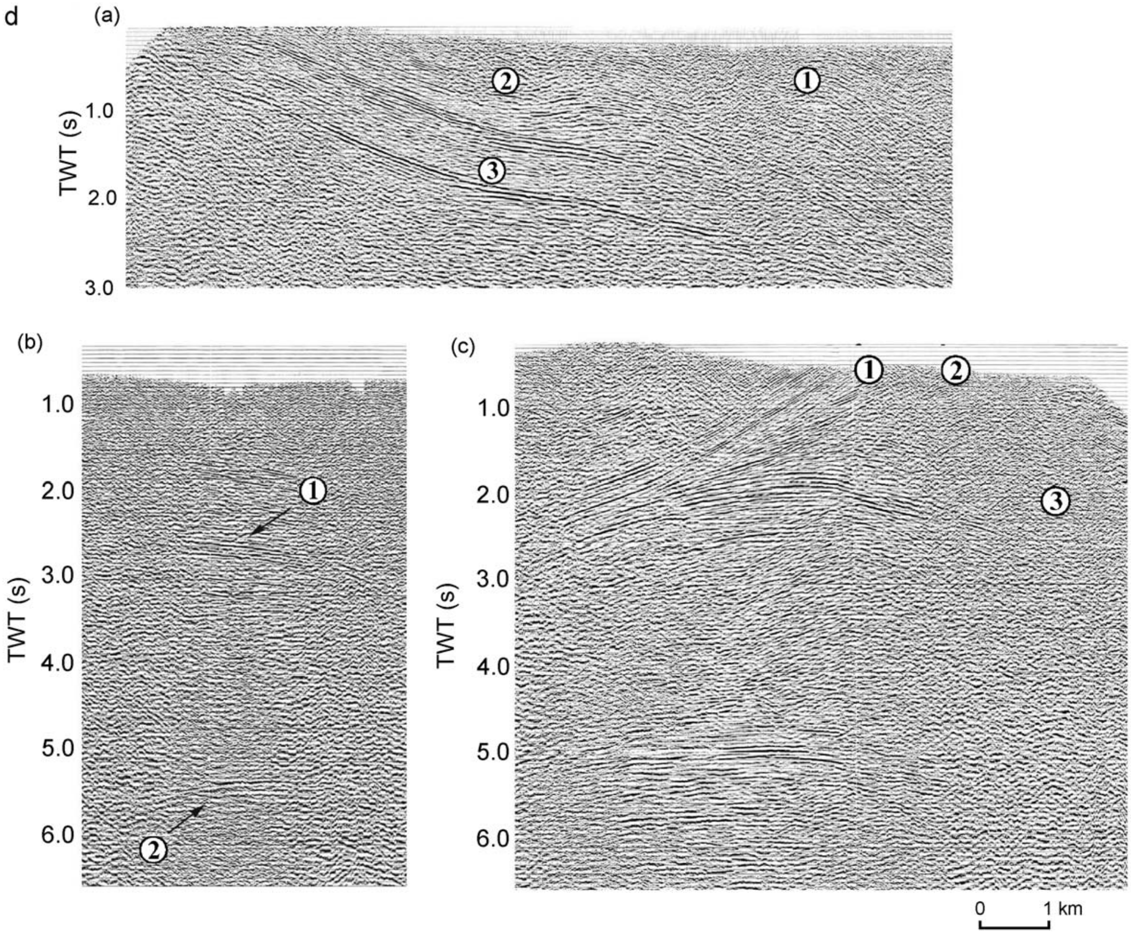

Fig. 6. Anticlines and detachment faults imaged in the common-depth-point (CDP) stacked seismic section of the MNS9601 profile. (a) The Qingshuihe (Qigu) anticline, where ① is the Qingshuihe thrust, ② and ③ are the Qingshuihe South thrusts; (b) detachments beneath the city of Dongwan (Fig. 4), where ① is the first detachment, and ② is the main detachment; (c) the Manas anticline (Fig. 4), which consists of the upper anticline (thrusts ① and ②) and the lower anticline (thrust ③); (d) all three seismic reflection sections without interpretive lines. Data quality is high.

well-imaged anticline between the two sets of reverse faults. This is the Qingshuihe anticline, which is part of the Qigu reverse fault/fold belt.

The central portion of the reflection profile (Fig. 6c) images the Manas anticline that actually consists of two separate shallow crustal anticlines, an upper and a lower anticline. Two south-dipping reverse faults, with dip angles of 60–70°, are imaged respectively on the southern and northern flanks of the more southerly anticline (thrusts ① and ②, Fig. 6c). The inclination of these reverse faults rapidly decreases with depth. The strong crustal deformation beneath the anticline is evidenced by a set of antiformal reflections. The second anticline, about 5 km to the north of the first anticline, is not visible at the surface (thrust ③, Fig. 6c).

The strong reflection events visible at 2.5–3.0- and 5.5–6.0-s TWT on the section (Fig. 6b and c) are interpreted as detachment surfaces, here called the first detachment and main detachment, respectively. The Manas listric fault merges into the first detachment at about 2.5-s TWT and joins the Qingshuihe reverse fault to the south. The reflections at 5.5–6.0 s on the southern portion of the profile probably correspond to the main detachment, which extends northward, where it appears to underlie the northernmost Manas anticline (Fig. 6b and c).

On the northern portion of the profile, in the Junggar basin, strong reflection events with good continuity appear at 2.0–2.5, 3.5–4.5 and 6.0–6.5 s on the section. These are most likely related to a set of sedimentary layers that reach a maximum depth of about 14 km. However, a clear image of the reflection events between Shihezi and Moguhu Lake (Figs. 4 and 5) only appears at about 4.5 s, and this image disappears beneath Moguhu Lake. A lateral discontinuity and/or offset of a strong package of reflections often indicates the existence of a fault. A blind thrust can be only weakly inferred north of Shihezi. This may be the eastward extension of the Dushanzi–Anjihai fold belt (Fig. 1b).

4.2. Lower crust

The top of the lower crust corresponds to a band of reflections at 10–11-s TWT on the seismic section (Fig. 5). The seismic section can be divided into a northern and a southern portion at the city of Shihezi. The image of the northern portion is quite simple, and the reflection events have strong energy and good lateral continuity. The image of the southern portion is somewhat more complex. In this portion, the reflections dip slightly southward, but their energy is generally weak, and there is little lateral continuity. The increase in crustal thickness along the profile is mainly attributable to an increase in the thickness of the lower crust.

4.3. Crust–mantle transition

Reflections, here interpreted as coming from the Moho, are clearly recorded at ~14 s (~40–45-km deep) on the northern portion of the profile (Fig. 5). The Moho reflections deepen to 16–17 km (~50–55-km deep) along the southern end of the seismic profile. These crustal thickness estimates are consistent with previous measurements in this region [25,26]. The Moho reflection is somewhat less pronounced on the southern portion of the profile. The crust–mantle transition may consist of a narrow (1–2 km) zone with a set of thin layers with alternating high and low seismic velocities, as suggested by numerical modeling of the seismic nature of the continental Moho by Sandmeier and Wenzel [27]. The steep dip of the Moho reflection south of Shihezi (Fig. 5) documents abrupt southward crustal thickening.

5. Crustal structure based on Bouguer gravity data and DSS data

At the northern margin of the eastern Tien Shan lies the Ürümqi piedmont depression, which is characterized by a negative Bouguer gravity anomaly. Along our seismic reflection profile, in the piedmont of the Tien Shan, the Bouguer gravity anomaly is about −210 mgal (Fig. 7a). North of the Qingshuihe anticline, the gravity anomaly reaches its minimum value, about −230 mgal. Near the structural zenith of the Manas anticline there is a modest gravity high (−215 mgal). The gravity anomaly increases gradually to the north of Shihezi to about −185 mgal at the end of the profile. The gravity lows along the profile correspond to low-density sediments of Mesozoic and Cenozoic age. There are additional gravity lows that are probably due to thickness variation or the drape folds of the piedmont sedimentary layers.

Guided by the crustal structure derived from the reflection profile, we constructed an initial crustal density model that was refined by performing a forward inversion of the Bouguer gravity data (Fig. 7b). The Cenozoic sediments were modeled with a density of 2400–2480 kg·m^{-3}. As noted above, the thickness of this sedimentary layer varies significantly along the reflection profile. These sediments are about 6-km thick at the northern end of the profile, and thin somewhat at the Manas anticline, finally vanishing at the Qingshuihe anticline. The local gravity high at the structural zenith of the Manas anticline then corresponds to the thinning of the Cenozoic sediments at this location. We conclude, based on the seismic and gravity models, that regionally the crust undergoes southward thickening some 30 km north of the Tien Shan, beneath the southern Junggar basin.

A nearly north–south trending deep seismic sounding (DSS) profile is located about 80 km west of the reflection profile [28] (Zhang X.K., personal

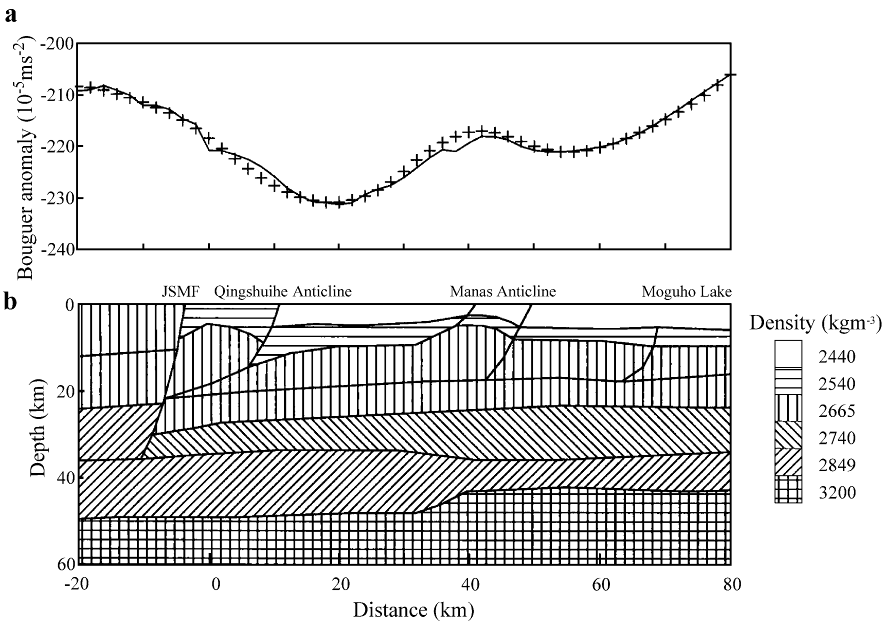

Fig. 7. Crustal density model extending from the northern Tien Shan to the Junggar basin along the transect route of the seismic reflection profile (Fig. 4). (a) Bouguer gravity anomalies, ranging from − 230 to − 190 mgal; (b) crustal density model showing modest crustal thinning from south to north. The MSN9601 seismic reflection profile corresponds to the distance between 0 and 80 km.

communication, 1999). The central portion of the DSS profile also crosses the Ürümqi piedmont depression, thus imaging the same geologic setting. On the record section of shot point Kuitun-south (Fig. 8a), one can clearly detect: (1) the refraction phase Pg from the basement, (2) three additional intra-crustal reflection phases (P_1, P_2 and P_3), and (3) the reflection phase PmP from the Moho discontinuity [29]. Phase P_1 exists only over a short distance, while P_2 is more persistent. Phase P_3 is reflected from the top of the lower crust (Fig. 8a). Two-dimensional synthetic seismograms [30] were used to forward-model the record section.

The final crustal model shows that the depth to the basement decreases from about 12 km beneath the shot point to about 5 km some 60 km south of the shot point. The depth to the C_2 and C_3 interfaces are 18 and 28 km, respectively (Fig. 8d). The Moho is at a depth of 50–55 km, the same as reported beneath the western and central Tien Shan [31], where elevations are generally much higher. Basement rocks along the DSS profile are composed of Jurassic sandstone, shale and coal-bearing strata. The interpretation of seismic amplitudes in the DSS record section suggests that a low-velocity layer exists beneath interface C_2 (Fig. 8d). This low-velocity layer is a stratum that may detach under the ambient north–south trending tectonic stress. The basement (interface "Pg"; Fig. 8d) and the top of the middle crust (interface C_2) can be correlated with the respective events at 2.5–3.0 and 5.5–6.0 s on the seismic reflection section (Fig. 5).

6. Analysis of tectonic deformation

Compressional orogenesis is a fundamental tectonic process that has played a major role in the development of central Asia, including the Tien Shan (e.g. [4,7,15]). Although deep seismic reflection images of compressional orogenic belts around the world differ considerably from each other, some common structural features are observed [32]. These common features include detachment and high-angle reverse faults and, in the middle crust, tectonic wedging [33]. Such structures are also visible on our seismic reflection profile.

Our model for the crustal structure and style of deformation in this study area (Fig. 9a) incorporates

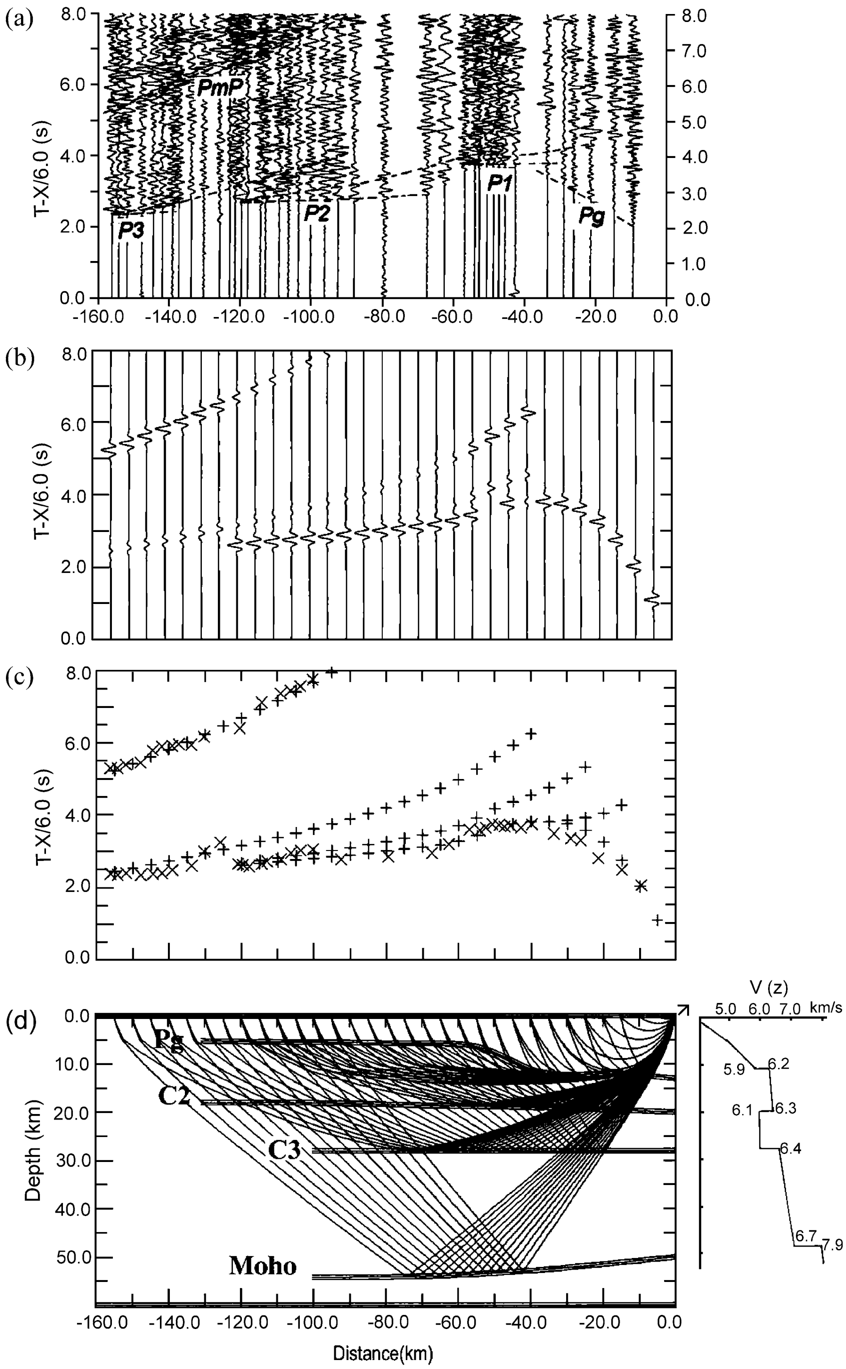

Fig. 8. Record section of shot point Kuitun-south on the deep seismic sounding profile (Fig. 1b) and interpreted using 2D ray-tracing and synthetic seismograms. (a) Record section with normalized trace, where the main phases are marked. Pg is the refracted arrival from the crystalline basement; P_1, P_2, and P_3 are intra-crustal reflections, and PmP is the reflection from Moho at a depth of 50–55 km. (b) Trace-normalized synthetic record section. (c) Observed and calculated travel time, where crosses and pulses denote respectively the observed and calculated travel time. (d) Ray paths and final crustal model. Crustal velocities are indicated on the right (c.f., [28]).

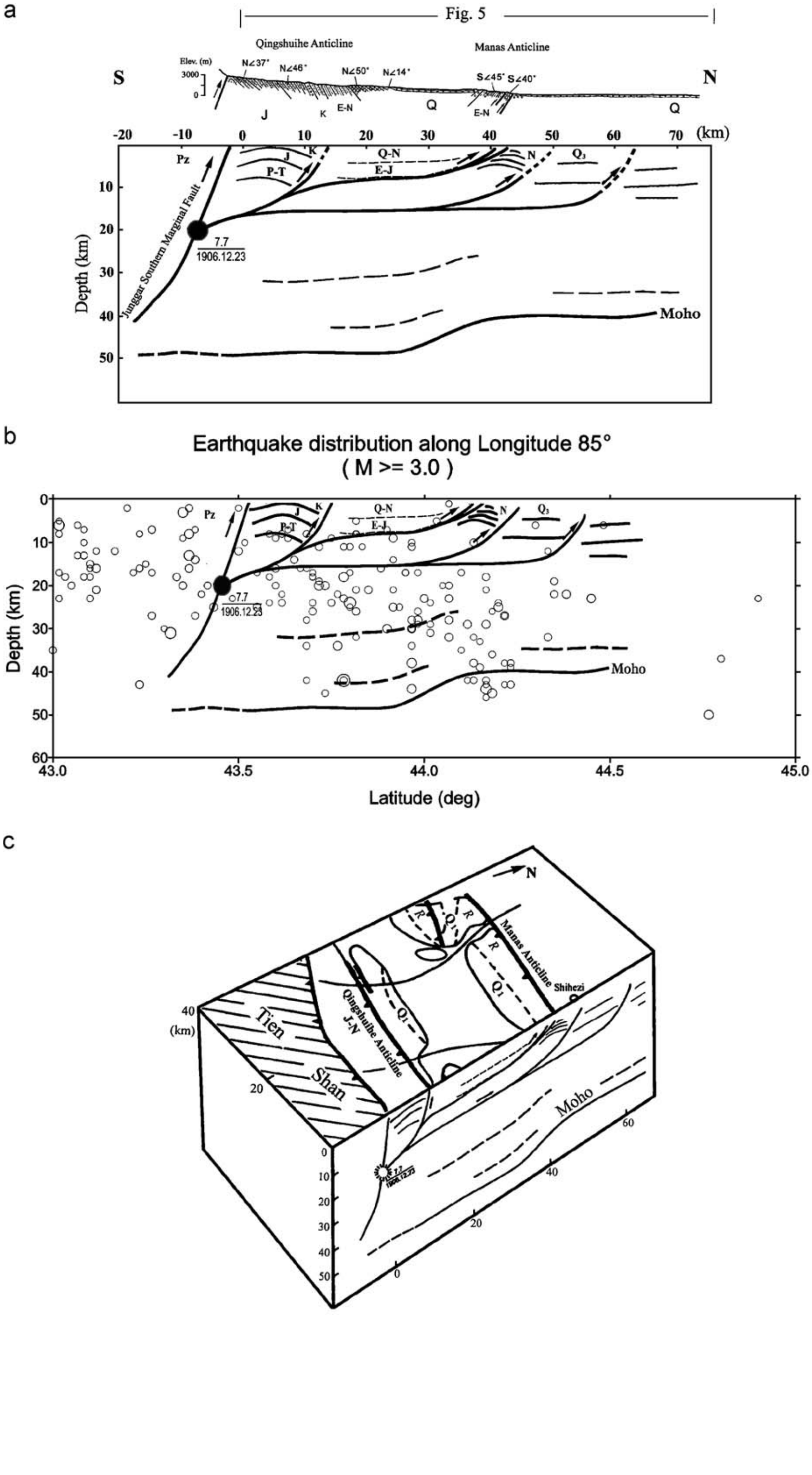
a
Fig. 5
Qingshuihe Anticline
Manas Anticline
S
N
Elev. (m)
3000
0
N∠37°
N∠46°
N∠50°
N∠14°
S∠45°
S∠40°
J
K
E-N
Q
E-N
Q
-20
-10
0
10
20
30
40
50
60
70
(km)
Pz
J
K
P-T
Q-N
E-J
N
Q₃
Junggar Southern Marginal Fault
7.7
1906.12.23
Depth (km)
10
20
30
40
50
Moho
b
Earthquake distribution along Longitude 85°
(M >= 3.0)
Depth (km)
Latitude (deg)
43.0
43.5
44.0
44.5
45.0
Moho
c
N
Tien
Shan
Qingshuihe Anticline
J-N
Manas Anticline
Shihezi
Q₁
R
Moho
40
(km)
20
60
7.7
1906.12.23

previous geologic mapping, the interpretation of the seismic reflection profile, and the crustal velocity structure determined from the DSS profile located 80 km to the west. The northern edge of the Tien Shan is marked by the Junggar Southern Marginal Fault (JSMF), here interpreted to be a high-angle reverse fault (Fig. 9a). To the north, a south-dipping fault is clearly imaged beneath the Qingshuihe anticline. We interpret this fault as a listric fault that becomes sub-horizontal as a detachment surface at a depth of 16 km (i.e. at the same depth as the seismic low-velocity zone identified on the DSS profile). A low angle fault is also imaged beneath the Manas anticline. Between the two anticlines, seismic reflections are observed at depths of 2.5–3.0 and 5.5–6.0 s (Fig. 5). These reflections are interpreted as the two detachment surfaces mentioned previously. This tectonic model is consistent with previous observations of detachment faulting in other compressional regimes within China, including the North China Basin [34], the Qinling-Dabei belt, and the Himalayan orogen [35].

The stacked seismic section (Fig. 5) indicates shearing along the detachment surfaces that extends northward to the nappe thrusts in the piedmont depression. This interpretation is in accord with geologic mapping by Avouac et al. [15] and Burchfiel et al. [7] who infer thin-skinned deformation along the northern margin of the eastern Tien Shan. In particular, Burchfiel et al. [7] estimated ∼ 6 km of shortening across each of two anticlines located 50 km due east of the Manas anticline. We infer that the Manas anticline has likely accommodated a similar amount of shortening. As illustrated in Fig. 9a, we suggest that movement along the steeply south-dipping fault propagates northward, forming the first ramp and the Qingshuihe anticline. The sub-horizontal detachments at 7 and 16 km then propagate further northward to form the Manas anticline. Our model is shown with micro-earthquake hypocenters in Fig. 9b, however, the diffuse micro-seismicity does not delineate major structural boundaries. A 3D perspective in Fig. 9c of the high-angle reverse and two detachment faults summarizes our tectonic model, which is in accord with previous geologic inferences.

The steep dip of the Moho reflection south of Shihezi (Fig. 5) documents abrupt southward crustal thickening beneath this profile. We infer this thickening is due to compression between the Tien Shan and Junggar blocks. It is significant that this crustal thickening occurs more than 30 km north of the topographic expression of the Tien Shan. This important observation may indicate underthrusting of the Junggar block beneath the north-central Tien Shan.

7. Crustal structure at the Manas earthquake hypocenter

Focal depths estimated for the 1906 Manas earthquake vary between 12 and 30 km [20,36,37]. To better estimate the seismogenic depth range in this region, we examined hypocenter depth information for 110 ($M \geq 3.7$) well-located earthquakes that have occurred beneath the northern Tien Shan since 1980 [38]. The statistics for these earthquakes show that the median focal depth is about 20 km (Fig. 10). In addition, we note that the future process for most well-recorded continental earthquakes initiates near or at the brittle-ductile transition (typically at a depth of 15–20 km [39,40]; e.g., the following moderate and large earthquakes: 1978 Loma Prieta, CA; 1994 Northridge, CA; 1999 Chi-Chi, Taiwan; 2001 Kunlun Shan, China). Based on these observations, we hypothesize that the 1906 M~7.7 Manas earthquake may have initially ruptured at a depth of ∼ 20 km or greater. The epicentral location and magnitude of the Manas earthquake is not well constrained due to a lack of local seismic data from the time of the event (c.f., discussion in [7]). In addition, micro-seismicity

Fig. 9. (a) Structural model along the seismic reflection profile MNS9601. The 1906 Manas earthquake is inferred to have occurred on a high-angle reverse fault that connects to several subsidiary faults, including two sub-horizontal detachments. Slip may have occurred on these detachments during the 1906 event, giving rise to surface deformation as far away from the main shock as the Manas anticline. (b) Structural model with hypocenters (Earthquake Catalogue of the Xinjiang Regional Seismological Bureau; G.M. Zhang, personal communication, 2003) superimposed; due to limited station coverage, there is considerable uncertainty regarding depths due to the sparseness of the local seismic network; nevertheless, there is abundant micro-seismicity throughout the crust, not only on the faults identified in the seismic reflection profile. (c) 3-D sketch of the crustal structure in the northeastern Tien Shan margin. Crustal shortening is accommodated by a combination of high-angle reverse and detachment faulting.

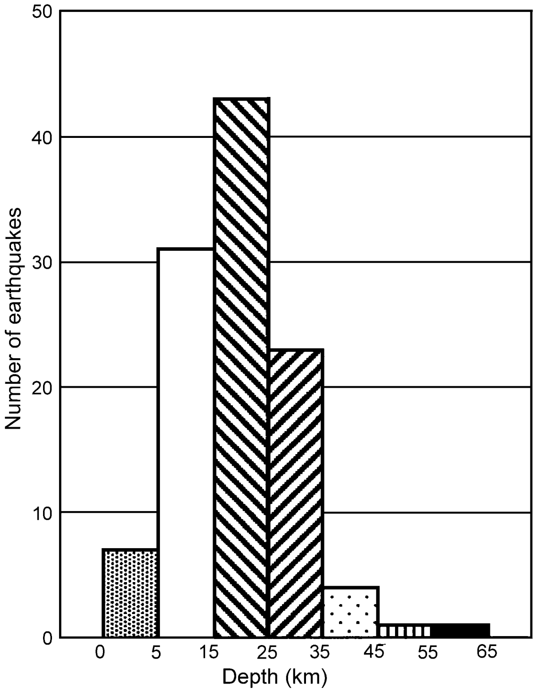

Fig. 10. Histogram of focal depths from 110 well-located earthquakes with $M \geq 3.7$ that have occurred in the northern Tien Shan margin since 1980. Seismicity is evident to depths as great as 60 km, with most events at about 35 km. Based on the depth distribution and a comparison with other large continental earthquakes (see text), we infer that the Manas 1906 M~7.7 event may have initiated at about 20-km depth or more.

often does not coincide with the location of large earthquake ruptures. For example, in the Tien Shan, present-day micro-earthquake activity is concentrated close to the southern margin of the Junggar basin, 15 km southwest of the inferred hypocenter of the 1906 Manas earthquake. This difference in location may be due to slip on the main detachment surface during the 1906 event. Thus, we hypothesize that the focal location of the Manas earthquake was at the intersection of the Junggar Southern Margin Fault and the detachment surface (Fig. 9a and c).

The regional structure imaged by our seismic reflection profile suggests that the Manas rupture may have propagated northwards to the Qingshuihe anticline. Field evidence indicates that strong shaking was felt over a large area (i.e., the Bourtongu-Shichang region). The Manas earthquake generated ground deformation, folding, and uplift about 45 km from the focus. Surface deformation related to the Manas earthquake includes steep scarps and a 130-km-long co-seismic uplift that formed along the Manas anticline [21] (Fig. 4). Based on these observations, we infer that slip initiated on the main reverse fault and continued onto the detachment faults imaged in this study at 7- and 16-km depth up to the Manas anticline. In recent years, studies of the 1980 El Assam earthquake in Algeria and the 1983 Coalinga earthquake in California have identified them as being generated by reverse faulting [41–43]. This kind of slip is accompanied by folding of the sort observed in the area of the 1906 Manas earthquake.

8. Conclusions

The 2500-km-long Tien Shan is the product of two Paleozoic collisional events, one along the southern margin involving the Tarim block, and the second along the northern margin involving the Kazakh platform (e.g., [2]). Following a long period of quiescence in the Mesozoic and early Cenozoic, the Tien Shan was reactivated in the middle to late Miocene as a result of the collision of India with southern Asia. The style of deformation in the Tien Shan has been well documented by geologic mapping [6–10,15,22] and earthquake focal mechanism studies [16,17,19]. The seismic profile presented in this paper provides an excellent image of the coupled reverse and detachment faults associated with the shortening of the crust in the transition zone between the northeastern Tien Shan and the southern Junggar Basin. Crustal thickness beneath the eastern Tien Shan is 50–55 km, the same as the western and central Tien Shan [31] despite the significantly lower elevations in the eastern Tien Shan. This implies that there is less upper mantle buoyancy (i.e., colder mantle) beneath the eastern Tien Shan.

We have shown evidence in a seismic reflection profile for two detachment faults at a depth of 7 and 16 km beneath the northern piedmont of the northeastern Tien Shan. The main detachment surface at 16-km depth converges with a steep angle reverse fault, the Junggar Southern Marginal Fault. We hypothesize that the M~7.7 1906 Manas earthquake occurred mainly on this reverse fault, with associated slip on the detachment faults beneath the southern

Junngar basin. Compression between the Tarim and Junggar blocks has resulted in a high level of seismicity, the uplift of the Tien Shan, and the creation of high-angle reverse faults and upper-crustal detachments that accommodate crustal shortening and thickening. Significantly, we find that the crust thickens by about 10 km some 30 km north of the topographic expression of the Tien Shan (i.e., beneath the southern Junggar basin). We infer from this observation that the crust of the Junggar basin may bend and underthrust the Tien Shan. These and similar structures within the 2500-km-long Tien Shan account for a significant fraction of the present-day shortening between India and Siberia.

Acknowledgements

The authors are grateful to Ding, G.Y., Wang, Y.P., Liu, G.D., Deng, Q.D., and Zhan, P.Z. of the China Seismological Bureau, and Ma, Y.J., and Xu, X. of the National 305 Project Office of the Xinjiang Uygur Autonomous Region of China for their valuable suggestions. Data collection in the field was assisted by the Sichuan Mountains Oil Seismics Company. This study is jointly supported by the State Natural Scientific Foundation of China (grant no. 49734240) and the China Seismological Bureau in the project 95-04-09. We wish to express our thanks to them. Detailed reviews by an anonymous reviewers, Jean-Phillipe Avouac, Eric Calais, Shane Detweiler, Francis Wu, and Scott King greatly improved the paper. ***[SK]***

References

[1] A.M.C. Sengor, Tectonic subdivisions and evolution of Asia, Bull. Tech. Univ. Istanb. 40 (1987) 355–435.

[2] B.F. Windley, M.B. Allen, C. Zhang, Z.-Y. Zhao, G.R. Wang, Paleozoic accretion and Cenozoic redeformation of the Chinese Tien Shan Range, central Asia, Geology 18 (1990) 128–131.

[3] P. Molnar, P. Tapponnier, Tectonics of Asia: consequences and implications of a continental collision, Science 189 (1975) 419–426.

[4] P. Tapponnier, P. Molnar, Active faulting and Cenozoic tectonics of the Tien Shan, Mongolia, and Baykal regions, J. Geophys. Res. 84 (1979) 3425–3459.

[5] E.R. Sobel, T.A. Dumitru, Thrusting and exhumation around the margins of the western Tarim basin during the India–Asia collision, J. Geophys. Res. 102 (1997) 5043–5063.

[6] A. Yin, S. Nie, P. Craig, T.M. Harrison, F.J. Ryerson, X.L. Qian, G. Yang, Late Cenozoic tectonic evolution of the southern Chinese Tian Shan, Tectonics 17 (1998) 1–27.

[7] B.C. Burchfiel, E.T. Brown, Q.D. Deng, X.Y. Feng, J. Li, P. Molnar, J.B. Shi, Z.M. Wu, H.C. You, Crustal shortening on the margins of the Tien Shan, Xinjiang, China, Int. Geol. Rev. 41 (1999) 665–700.

[8] M.B. Allen, S.J. Vincent, P.J. Wheeler, Late Cenozoic tectonics of the Kepingtage thrust zone: interactions of the Tien Shan and the Tarim Basin, northwest China, Tectonics 18 (1999) 639–654.

[9] M.E. Bullen, D.W. Burbank, J.I. Garver, K.Ye. Abdrakhmatov, Late Cenozoic tectonic evolution of the northwestern Tien Shan: new age estimates for the initiation of mountain building, Geol. Soc. Am. Bull. 113 (2001) 1544–1559.

[10] M.E. Bullen, D.W. Burbank, J.I. Garver, Building the northern Tien Shan: Integrated thermal, structural, and topographic constraints, J. Geol. 111 (2003) 149–165.

[11] J.M. Sun, R.X. Zhu, J. Bowler, Timing of the Tienshan Mountains uplift constrained by megnetostratigraphic analysis of molasses deposits, Earth Planet. Sci. Lett. 219 (2004) 239–253.

[12] Q. Wang, D. Guoyu, Q. Xuejun, W. Xiaoqiang, Y. Xinzhao, Recent rapid shortening of crust across the Tienshan Mts., and relative motion of tectonic blocks in the north and south, Chin. Sci. Bull. 45 (2000) 1995–1999.

[13] C. Reigber, G.W. Michel, R. Galas, P. Angermann, J. Klotz, J.Y. Chen, A. Papschev, et al., New space geodetic constraints on the distribution of deformation in Central Asia, Earth Planet. Sci. Lett. 191 (2001) 157–165.

[14] W.E. Holt, N. Chamot-Rooke, X. Le Pichon, et al., Velocity field in Asia inferred from Quarternary fault slip rates and Global Positioning System observations, J. Geophys. Res. 105 (2000) 19185–19209.

[15] J.-P. Avouac, P. Tapponier, M. Bai, H. You, G. Wang, Active thrusting and folding along the northern Tien Shan and Late Cenozoic rotation of the Tarim relative to Dzungaria and Kazakhstan, J. Geophys. Res. 98 (1993) 6755–6804.

[16] J. Ni, Contemporary tectonics in the Tien Shan region, Earth Planet. Sci. Lett. 41 (1978) 347–354.

[17] M.R. Nelson, R. McCaffrey, P. Molnar, Source parameters for 11 earthquakes in the Tien Shan, Central Asia, determined by P and SH waveform inversion, J. Geophys. Res. 92 (1987) 12629–12648.

[18] X.Y. Feng, Q.D. Deng, J.B. Shi, J. Li, H.C. You, Y. Zhang, G.H. Yu, Z.M. Wu, Active tectonics of the southern and northern Tien Shan and its tectonic evolution, Editorial Board of Research on Active Fault, Research on Active Fault, vol. 1, Seismological Press, Beijing, 1991, pp. 1–16, in Chinese.

[19] S. Ghose, R.J. Mellors, A.M. Korjenkov, M.W. Hamburger, T.L. Pavlis, G.L. Pavlis, M. Omuraliev, E. Mamyrov, A.R. Muraliev, The Ms = 7.3 1992 Suusamyr, Kyrgystan, earthquake in the Tien Shan: 2. Aftershock focal mechanisms

and surface deformation, Bull. Seismol. Soc. Am. 87 (1997) 23–38.

[20] G.X. Gu, Catalog of Chinese Earthquakes (1831 BC ~ AD 1969), Science Press, Beijing, 1983, pp. 200–201, in Chinese.

[21] P.Z. Zhang, Q.D. Deng, X.W. Xu, S.Z. Peng, X.Y. Feng, X.P. Yang, R.B. Zhao, J. Li, Blind thrust, folding earthquake, and the 1906 Manas earthquake, Xinjiang, Seismology and Geology 16 (1994) 193–203 (in Chinese).

[22] Q.D. Deng, X.Y. Feng, P.Z. Zhang, X.W. Xu, X.P. Yang, S.Z. Peng, Paleoseismology in the northern piedmont of the Tienshan Mountains, northwestern China, J. Geophys. Res. 101 (1996) 5895–5920.

[23] Seismological Bureau of Xinjiang Uygur Autonomous Region, Compilation of Seismic Data in Xinjiang Uygur Autonomous Region, Seismological Press, Beijing, 1985, pp. 38–44, in Chinese.

[24] Compilation Group for Deep Geophysics, State Seismological Bureau, Geophysical Exploration of Crust and Upper Mantle in China, Seismological Press, Beijing, 1986, pp. 243–244, in Chinese.

[25] S. Li, W.D. Mooney, Crustal structure of China from deep seismic sounding profiles, Tectonophysics 288 (1998) 105–113.

[26] Y.X. Wang, W.D. Mooney, X.C. Yuan, R. Coleman, The crustal structure from the Altai mountains to the Altyn Tagh fault, northwestern China, J. Geophys. Res. 108 (article 2322).

[27] K.J. Sandmeier, F. Wenzel, Synthetic seismograms for a complex crustal model, Geophys. Res. Lett. 13 (1986) 22–25.

[28] J.M. Zhao, G.D. Liu, Z.X. Lu, X.K. Zhang, G.O. Zhao, Lithospheric structure and dynamic processes of the Tienshan orogenic belt and the Junggar basin, Tectonophysics 376 (2003) 199–239.

[29] J.M. Zhao, J. Tang, H.J. Zhang, C.K. Zhang, J. Yang, S.X. Jia, J.S. Zhang, Z.X. Yang, Wavelet transform and its application in data processing and interpretation of seismic reflection/refraction profile, Chin. J. Geophys. 43 (2000) 666–676 (in Chinese).

[30] V. Cerveny, I. Psencik, SEIS83-numerical modeling of seismic wavefield in 2-D laterally varying layered structures by the ray method, in: E.R. Engdahl (Ed.), Documentation of Earthquake Algorithm, Rep. SE-35, World Data Center for Solid Earth Geophysics, Boulder, CO, 1984, pp. 36–40.

[31] S.W. Roecker, T.M. Sabitova, L.P. Vinnik, A. Burmakov, M.I. Golvanov, R. Mamatkanova, L. Munirova, Three-dimensional elastic wave velocity structure of the western and central Tien Shan, J. Geophys. Res. 98 (1993) 15779–15795.

[32] W.D. Mooney, R. Meissner, Multi-genetic origin of crustal reflectivity: A review of seismic reflection profiling of the continental lower crust and Moho, in: D.M. Fountain, A. Arculus, R. Kay (Eds.), The Continental Lower Crust, Elsevier, New York, 1992, pp. 39–52.

[33] R. Meissner, T. Wever, P. Sadowiak, Continental collisions and seismic signature, Geophys. J. Int. 105 (1991) 15–23.

[34] C.Y. Wang, X.K. Zhang, Q.J. Wu, Z.P. Zhu, Seismic evidence for detachment in the North China Basin, Chin. J. Geophys. 37 (1994) 611–619.

[35] W.J. Zhao, K.D. Nelson, Deep seismic-reflection evidence for continental underthrusting beneath southern Tibet, Nature 366 (1993) 557–559.

[36] Y.S. Xie, M.B. Cai, Compilation of Historical Earthquake Data in China, vol. 4, Science Press, Beijing, 1986, pp. 6–7, next book (in Chinese).

[37] M.B. Department of Seismic Hazard Prevention, State Seismological Bureau, Catalog of Destructive Earthquakes in the World (2150 BC ~ AD 1991), Seismological Press, Beijing, 1996, pp. 82–83, in Chinese.

[38] Q.L. Li, R. Song, J.B. Chen, Summary Catalog of Chinese Earthquakes of Different Historical Periods, Seismological Press, Beijing, 1991, pp. 80–104, in Chinese.

[39] R.H. Sibson, Fault zone models, heat flow, and the depth distribution of earthquakes in the continental crust of the United States, Bull. Seismol. Soc. Am. 72 (1982) 151–163.

[40] S. Das, C.H. Scholz, Why large earthquakes do not nucleate at shallow depths, Nature 305 (1983) 621–623.

[41] R.S. Stein, R.S. Yeats, Hidden earthquakes, Sci. Am. 260 (1988) 48–57.

[42] G.C.P. King, C. Vita-Finizi, Active folding in the Algerian earthquake of 10 October 1980, Nature 292 (1981) 22–26.

[43] R.S. Stein, G.C.P. King, Seismic potential revealed by surface folding: 1983 Coalinga, California, earthquake, Science 224 (1984) 869–872.

[44] Z.H. Xu, S.Y. Wang, Y.R. Huang, A.G. Gao, The tectonic stress field of Chinese continent deduced from a great number of earthquakes, Acta Geophys. Sin. 32 (1989) 636–647 (in Chinese).

[45] X.Y. Ma, Lithospheric Dynamics Atlas of China, Cartographic Publishing House, Beijing, 1989. 57 pp.

[46] K.Y. Abdrakhmatov, S.A. Alddazhanov, B.H. Hager, M.W. Hamburger, T.A. Herring, et al., Relatively recent construction of the Tien Shan inferred from GPS measurement of present-day crustal deformation rates, Nature 384 (1996) 450–453.